W416–W423 *Nucleic Acids Research, 2016, Vol. 44, Web Server issue* *Published online 5 May 2016*
doi: 10.1093/nar/gkw368

BetaSCPWeb: side-chain prediction for protein structures using Voronoi diagrams and geometry prioritization

Joonghyun Ryu[1], Mokwon Lee[1], Jehyun Cha[1], Roman A. Laskowski[2], Seong Eon Ryu[3] and Deok-Soo Kim[4,*]

[1]Vorononi Diagram Research Center, Hanyang University, Korea, [2]European Bioinformatics Institute, Wellcome Trust Genome Campus, UK, [3]Department of Bioengineering, Hanyang University, Korea and [4]School of Mechanical Engineering, Hanyang University, Korea

Received February 5, 2016; Revised April 22, 2016; Accepted April 23, 2016

ABSTRACT

Many applications, such as protein design, homology modeling, flexible docking, etc. require the prediction of a protein's optimal side-chain conformations from just its amino acid sequence and backbone structure. Side-chain prediction (SCP) is an NP-hard energy minimization problem. Here, we present BetaSCPWeb which efficiently computes a conformation close to optimal using a geometry-prioritization method based on the Voronoi diagram of spherical atoms. Its outputs are visual, textual and PDB file format. The web server is free and open to all users at http://voronoi.hanyang.ac.kr/betascpweb with no login requirement.

INTRODUCTION

The side-chain prediction (SCP) problem aims to predict a protein's side-chain conformations to minimize its total potential energy. It is useful for important applications such as protein design (1,2), homology modeling (3–5), flexible docking (6,7), etc. The conformations are usually selected from a rotamer library compiled from a statistical analysis of exprimentally determined protein structures. Given a rotamer library and a force field to define an energy function, the solution to an SPC-problem attempts to assign the optimal rotamer to each residue so that the total energy is minimized.

Consider a protein of n residues. Let $\mathcal{R} = \{R_1, R_2, \ldots, R_n\}$ be the set of rotamer sets where $R_i \in \mathcal{R}$ is a set of possible rotamer instances for the i-th residue. $\mathcal{R}$ can be defined using one of the popular rotamer libraries (8–10). Then, the SCP-problem involves choosing the optimal rotamer instance from R_i for all residues using a mathematical minimization formulation so that the entire energy of the protein structure is minimized. The SCP-problem is known to be NP-hard (11) and a heuristic approach is inevitable in its solution process. Examples of approaches used include DEE (Dead-end elimination) based approaches (12,13), mathematical programming based approaches (14,15), graph-theoretic approaches (16,17), Monte Carlo simulation (5), simulated annealing (18) and genetic algorithms (19).

This paper introduces a web server, BetaSCPWeb, which solves SCP-problems when a backbone is given. The server implements a significantly enhanced version of the earlier BetaSCP algorithm (20,21) in terms of both solution quality and computational efficiency. The fundamental idea behind BetaSCPWeb is that a structure's potential energy is correlated with the total volume of atomic intersections. The latter can be efficiently computed from the Euclidean proximity information contained in the Voronoi diagram of the 3D spherical atoms (22) and its beta-complex (23).

MATERIALS AND METHODS

Voronoi diagrams, quasi-triangulations and β-complexes

Let $S = \{s_1, s_2, \ldots, s_n\}$ be a set of three-dimensional spheres where $s_i = (c_i, r_i)$ has center c_i and radius r_i. The Voronoi cell of s_i is defined as $\mathcal{VC}(s_i) = \{d(x, c_i) - r_i < d(x, c_j) - r_j, i \neq j\}$ where $d(x, y)$ is the Euclidean distance between x and y. Then the *Voronoi diagram* $\mathcal{VD}$ of S is defined as the set of Voronoi cells for spheres in S. $\mathcal{VD}$ correctly reflects the size differences among spheres. Be aware that $\mathcal{VD}$ is different from the ordinary Voronoi diagram of atomic centers and it is this difference that facilitates the powerful features of BetaSCPWeb. The dual of $\mathcal{VD}$ is the *quasi-triangulation* $\mathcal{QT}$ whose topological entities are dual-mapped from those of $\mathcal{VD}$. $\mathcal{QT}$ is a generalization of the Delaunay triangulation in which $\mathcal{VD}$ is just the ordinary Voronoi diagram of points. See (22) for $\mathcal{VD}$, (24) for Voronoi diagrams in general, and (23,25–26) for $\mathcal{QT}$. Figure 1A shows $\mathcal{VD}$ and $\mathcal{QT}$

*To whom correspondence should be addressed. Tel: +82 2 2220 0472; Fax: +82 2 2292 0472; Email: dskim@hanyang.ac.kr

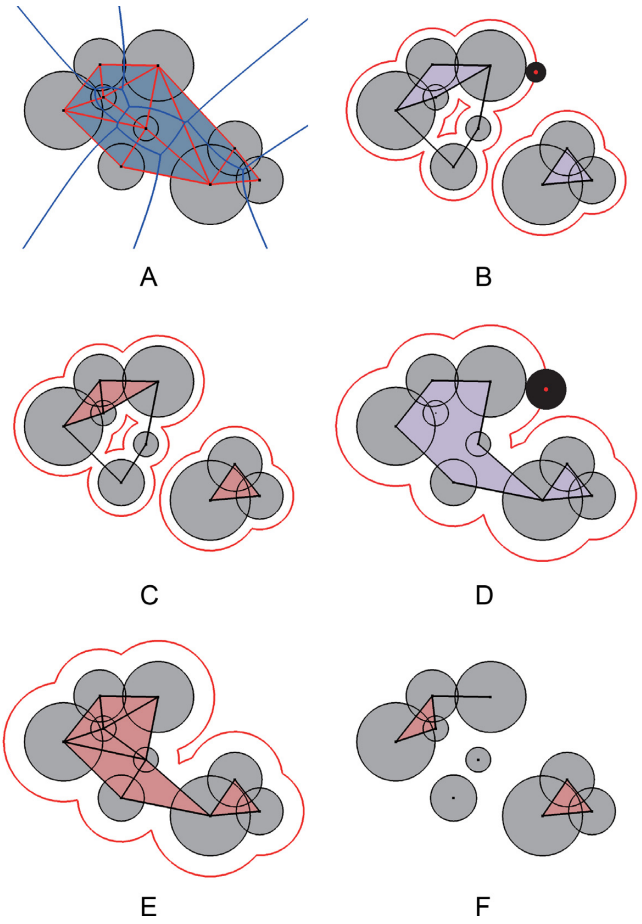

Figure 1. Voronoi diagram of 2D circular atoms and its derivative constructs (Figures drawn using BetaConcept (27)). (**A**) The Voronoi diagram (blue lines) of circles and its quasi-triangulation (red lines), (**B**) the β-shape (shaded polygon plus line segments) and corresponding offset (red curve) for a probe of radius $\beta_1 \geq 0$, (**C**) the corresponding β-complex (shaded triangles plus line segments) for β_1, (**D**) the β-shape (shaded polygon) and the offset (red curve) for $\beta_2 > \beta_1$, (**E**) the β-complex (shaded triangles) for β_2 and (**F**) the zero β-complex (shaded triangles plus line segments) for a β-probe of zero radius.

for a set of 2D circular atoms. $\mathcal{VD}$ can be computed in an $O(n)$ time on average for n spheres.

Suppose, we roll a circular probe (black disk) of radius $\beta_1 \geq 0$ over the atoms while keeping tangential contact with the boundary. Then, the trajectory of the probe center maps the red curve, called an offset, in Figure 1B. The polygonal shape in Figure 1B is called the *beta-shape* $\mathcal{BS}$ which contains the information to compute the offset and can be efficiently computed from $\mathcal{QT}$. The subset of $\mathcal{QT}$ that corresponds to $\mathcal{BS}$, as shown in Figure 1C, is called the *beta-complex* $\mathcal{BC}$ and contains the proximity information within and inside the boundary of the atom set while the boundary is defined by the probe with a particular radius. Figures 1D and E show their counterparts for $\beta_2 > \beta_1$. Figure 1F is called the zero beta-complex corresponding to the probe of zero radius and therefore it contains the intersection information among atoms. Figures 1A-1F are drawn using BetaConcept (27). We emphasize that $\mathcal{BC}$ and $\mathcal{BS}$ for an arbitrary β-value can be computed very efficiently through a binary search of the sorted simplex sets of $\mathcal{QT}$ (23). For example, $\mathcal{BS}$ can be computed in $O(\log m + k)$ time where $m = O(n)$ represents the number of entities in $\mathcal{QT}$ and $k < m$ the number of entities in $\mathcal{BS}$.

The BetaSCP algorithm

The BetaSCP algorithm consists of three steps: the initial assignment of rotamers to all residues (Step I), the improvement of the rotamer assignment via a combinatorial search (Step II) and the local optimization of the energy landscape (Step III). For Step I, BetaSCP chooses the most probable rotamers for all residues using the probabilities defined in the rotamer library. Figure 2A shows a short polypeptide and the clusters of possible rotamers for each residue, as obtained from a backbone independent rotamer library (8). Figure 2B shows an example of such an initial assignment.

Step II begins with the initial assignment of rotamers and improves this assignment by replacing each rotamer with a better one using a rapid geometric approximation of energy function. Given the initial rotamer assignment, a combinatorial search stage improves the solution by finding a better alternative to each initially assigned rotamer. Keeping the rotamers of the other residues fixed, we search for an alternative rotamer instance, r_ρ, for the current residue, ρ, from its rotamer instance set, R_ρ, in terms of the volume of intersection of r_ρ with the rest of the protein structure. The thesis is that the smaller the intersection, the lower the energy and thus the stabler the structure. In this way, the Voronoi diagram and beta-complex provide a significant method for accelerating the calculation. The procedure is repeated, residue by residue, for the entire protein, and then iterated a sufficient number of times until an *a priori* defined terminating condition is encountered. This completes the combinatorial search stage.

A justification for this approach is illustrated in Figure 3A. The dotted curve shows the Lennard-Jones (LJ) potential (left vertical axis) as a function of the distance between a carbon and an oxygen atom. The solid curve is the corresponding volume of intersection (right vertical axis) of the two atoms. The scales of the two vertical axes are immaterial as they are different units. What is important is that the two curves are similar, particularly around the distance of most frequent intersection in relatively stable protein structures where both curves are monotonically decreasing. At sufficient distance, where the intersection volume becomes null, the corresponding energy approaches zero. Figure 3B shows the relationship between these two curves: the LJ-energy versus the intersection volume. Hence, a rapidly calculated intersection volume can be used to estimate its corresponding energy using an *a priori* prepared mapping table. The significant deviation between the two curves when two atoms are close in Figure 3A is reflected by the sharp rise in the curve in Figure 3B. A similar observation holds for all other atom pairs.

If there is no intersection between two atoms, we consider the repulsive force does not apply any more but the attractive one does. In such a case, we use a modified form of the corresponding attraction term $\lambda B_{ij}/d^6$ where d and B_{ij} represent the distance between two atom centers and the LJ-coefficient corresponding to the two atoms, respectively,

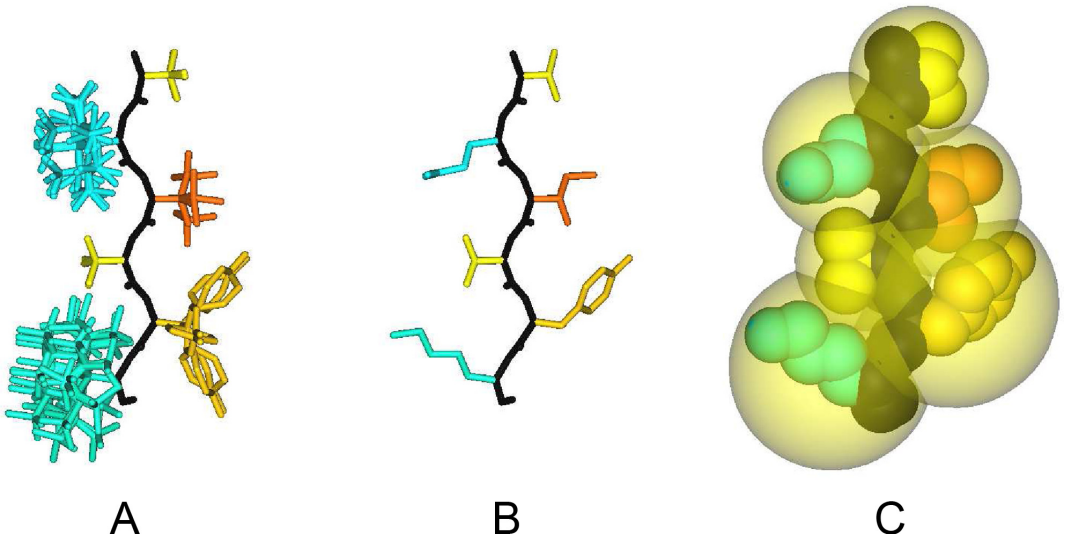

Figure 2. Overview of the BetaSCP algorithm: (**A**) a backbone fragment of an input protein structure (PDB accession code: 3fqp) with all possible rotamer instances for each residue from a backbone-independent rotamer library, (**B**) the fragment after a single rotamer has been assigned to each residue and (**C**) the structure of (B) as a space-filling model shown inside the minimum enclosing sphere of each residue.

and λ is an empirical coefficient intended to reflect the nature of van der Waals energy as much as possible in the BetaSCP algorithm.

The critical feature of BetaSCP is that the active use of the Voronoi diagram and beta-complex accelerates the computation by significantly reducing the search space. Figure 2C shows the minimum enclosing sphere (MES) of each residue together with its assigned rotamer. An efficient algorithm for computing the MES of a set of spheres is available (28). Given the MES of each residue, we can compute the Voronoi diagram and beta-complex corresponding to the probe of zero radius to identify intersecting MES pairs. This provides proximity information among the residues in the 3D Euclidean space that allows us to quickly filter out non-intersecting residues and hence obviate unnecessary intersection computation. This significantly reduces the search space. Note that, due to the powerful properties of the Voronoi diagram and beta-complex, this procedure does not sacrifice solution quality.

Remark. Let r_1 and r_2 be the radii of two atoms. Figure 3B shows a curve relating the LJ-potential with the intersection volume. As both curves in Figure 3A are monotonic in the interval $[0, r_1 + r_2)$, the range of center-to-center distances between two intersecting atoms, the curve in Figure 3B is also monotonic. In the figure, the horizontal axis is the intersection volume and the vertical axis the corresponding LJ-energy. Hence, given an atom pair separated by distance d, the energy of the atom pair can be quickly determined once the mapping table corresponding to Figure 3B is available.

Given the improved rotamers from the combinatorial search, Step III, i.e. the local optimization of the energy landscape, optimizes each rotamer dihedral angle. It uses the conjugate gradient method, as was also used by (17,29) to solve the nonlinear energy minimization problem for each residue in turn, considering only other residues in its Euclidean vicinity as identified using the beta-complex with a sufficiently large probe to include interactions with neighbors. Again, use of the β-complex both reduces the search space and improves the solution quality of the highly nonlinear programming formulation of the problem.

RESULTS AND DISCUSSION

The functions of BetaSCPWeb

The inputs to BetaSCPWeb consist of an amino acid sequence and the 3D coordinates of the backbone in PDB format. Alternatively, users may enter a PDB accession code (http://www.rcsb.org/pdb/). The program outputs the computed side-chain coordinates in PDB format, and also displays its results visually and in text form. BetaSCPWeb allows the user to choose rotamers from three different rotamer libraries: the most recent backbone-dependent one (10) in addition to the earlier backbone-independent and backbone-dependent libraries (8,9) .

An example of both visual and textual output is shown in Figure 4. The textual output summarizes the predicted structure, giving its energy, side-chain dihedral angles, and, where relevant, compares it to the input structure in terms of an RMSD (root-mean squared distance) and energy difference. Various computational statistics are also provided. The visual output, shown in Figure 4, depicts the predicted structure as a space-filling, ball-and-stick, stick, or line model using JSmol (30). BetaSCPWeb computes two versions of the protein structure prediction, both of which can be downloaded in PDB-format: one is toward the energy-optimized structure and the other toward the native structure.

The architecture of BetaSCPWeb

BetaSCPWeb consists of four components: (i) molecular geometry operating system (MGOS), (ii) backbone evaluator, (iii) intersection volume minimizer and (iv) energy

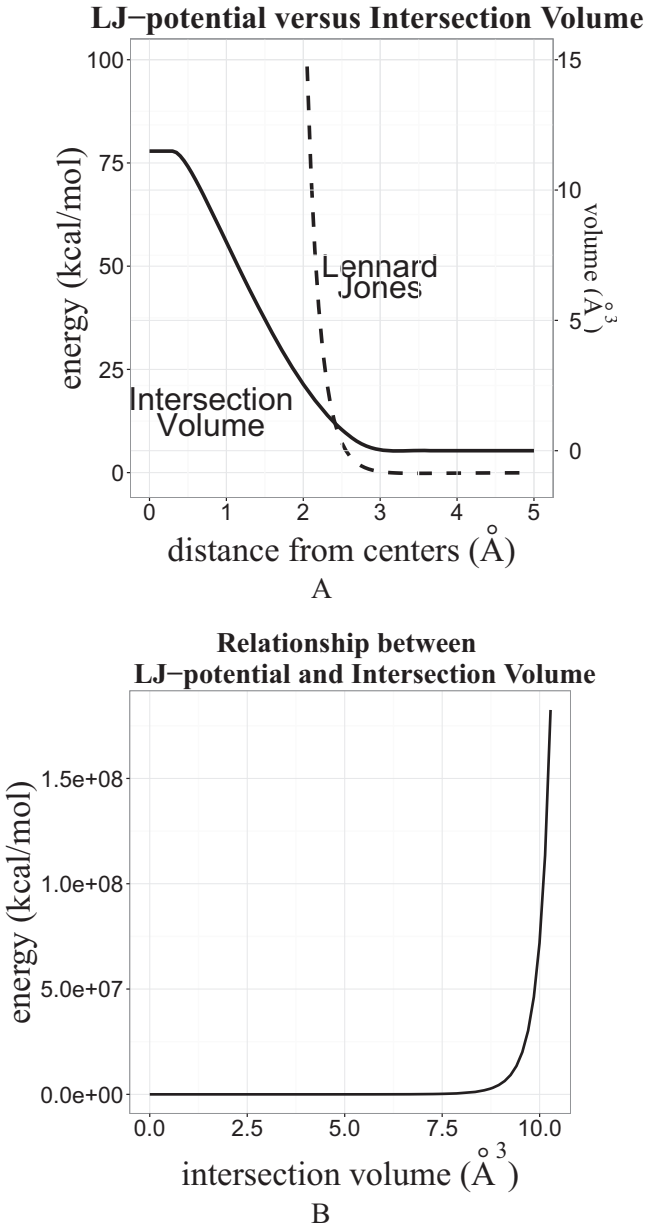

Figure 3. High correlation between the LJ-potential energy and intersection volume of a particular atom pair, carbon and oxygen, which is also observed for other atom pairs: (**A**) LJ-potential energy (dotted curve, left axis) and intersection volume (solid curve, right axis) between carbon and oxygen as a function of the distance between the two atoms. The vertical axes have been scaled to show that the two curves are highly correlated. (**B**) The graph of the deviation between the LJ-potential energy and the intersection volume

minimizer. Figure 5 shows how these components are connected: arrows denote computational and logic data flow. Given an input structure and a rotamer library, the backbone evaluator analyzes structural properties such as the dihedral angles of the backbone and side-chains and checks the amino acid sequence. Then, the best possible rotamer instance of each residue is obtained to complete Step I of the BetaSCP algorithm. The intersection volume minimizer assigns a rotamer to each residue by finding the rotamer with minimum intersection volume which eventually maps to the LJ-potential energy. Hence, it is the major computational component of Step II. The energy minimizer works for Step III to further improve the quality of protein structure by marginally modifying the side-chain dihedral angles via energy minimization. The MGOS computes the Voronoi diagram, transforms to a quasi-triangulation and extracts the beta-complex used to accelerate the computation of the intersection volume minimizer and energy minimizer. Therefore, MGOS is the infrastructure of the entire system. BetaSCPWeb obtains PDB files directly from the RCSB PDB web site upon user's entry of a PDB accession code (Figure 6).

Performance of BetaSCPWeb

BetaSCPWeb has been validated using the native structure set used by SCWRL4 (16), denoted by NAT-SCWRL4SET and the most recent backbone-dependent rotamer library (10). A benchmark test showed that BetaSCPWeb tended to consistently produce protein structures of lower energy in contrast to the energies returned by the popular SCWRL4 and CISRR programs (16,31) which tended to fluctuate markedly (Figure 7A). The computation times of all three methods were comparable (Figure 7B). Running BetaSCPWeb on 413 structures from the CASP contest (rounds 6–11) showed that it significantly improved the current CASP structures in terms of energy as shown in Figure 8, where E_{native} and E_{beta} denote the energy of the native structures from CASP and that of the predicted structures by BetaSCPWeb, respectively. On average, the predicted structures by BetaSCPWeb had about 7% lower energy than the CASP structures. Note that the computation time increase shows a strong linear behavior with respect to the problem size.

Two other important measures popular for assessment of predicted protein structures are RMSD and the percentage of correct side-chain angles (i.e. χ_1, χ_{1+2}, etc.) from some reference structure. While a usual practice is to use native structures as the reference structures, we observe that many native structures still have room for improvement from an energy point of view. We thus improved the native structures of NAT-SCWRL4SET to get an optimized structure set OPT-SCWRL4SET by applying an intensified variation of Step III several times as follows. We compute the MES for each residue including its side-chain. Then, we compute the Voronoi diagram of all MESs to quickly find the Euclidean neighbor Voronoi cells up to the second neighbor shells of each Voronoi cell. Then, we formulate and solve a nonlinear optimization problem of side-chain angles using the atoms in the neighbor shells. After changing the side-chain conformation according to the optimization solution, we compute the MES of the updated residue and compute the Voronoi diagram of all MESs once more. This process repeats for all residues to complete one iteration and we performed four iterations to get the structures of very low energy conformation in OPT-SCWRL4SET. Observe the difference of the energy levels between NAT-SCWRL4SET and OPT-SCWRL4SET in Figure 9

We computed the distribution of the deviation of the side-chain angles of each pair of corresponding structures

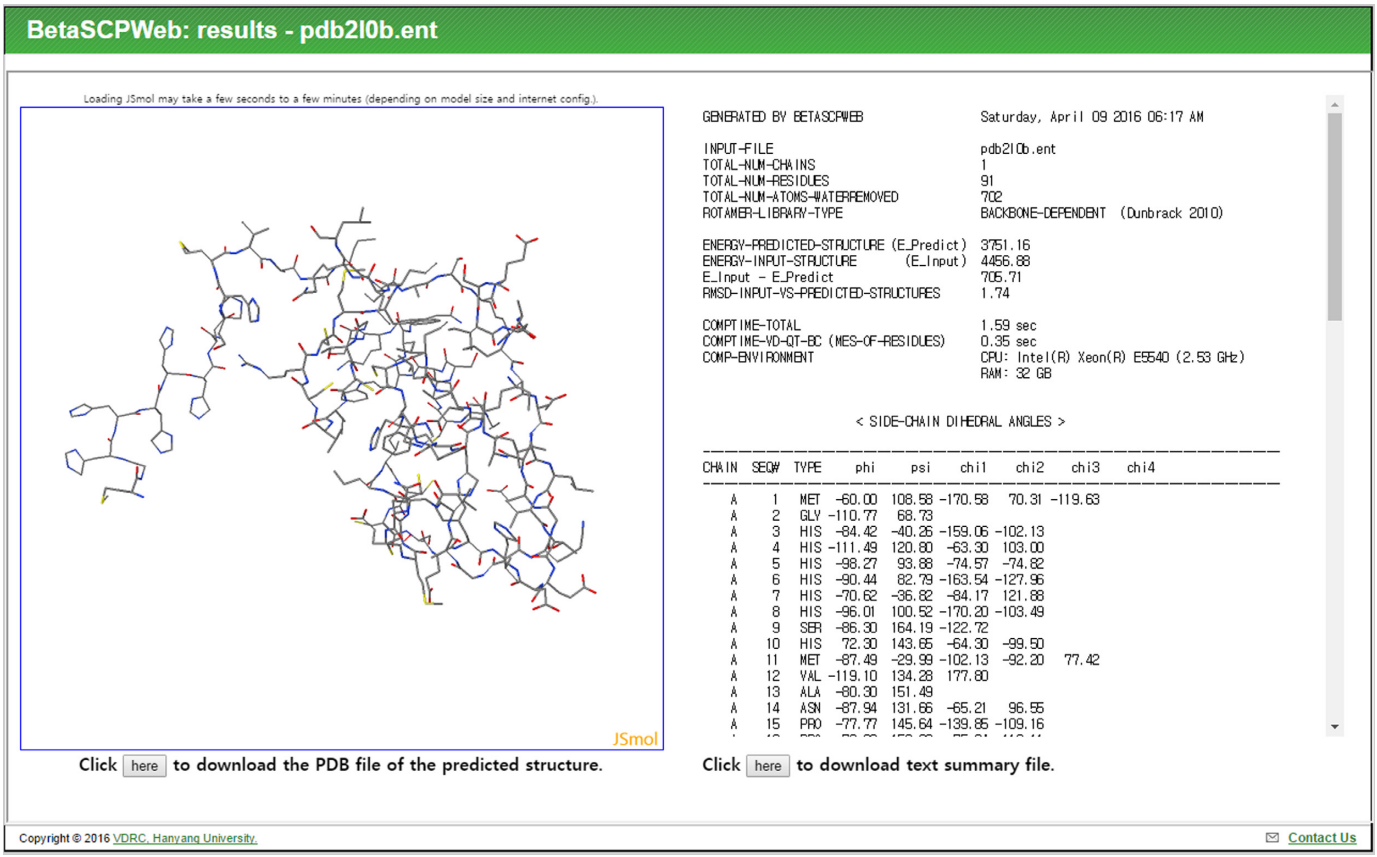

Figure 4. Screen shot of the output screen of BetaSCPWeb.

Table 1. Percent correct prediction rate of side-chain χ-angles (within 40° deviation) and RMSD (λ = 0.9): OPT-SCWRL4SET

		BetaSCPWeb (A)				CISRR (B)	SCWRL4 (C)
		I (A1)	I+II (A2)	I+III (A3)	I+II+III (A4)		
χ	χ_1	53.05%	52.06%	70.50%	68.72%	57.44%	57.33%
	χ_{1+2}	30.56%	38.59%	46.38%	50.47%	40.12%	40.17%
	χ_{1+2+3}	8.57%	13.50%	16.86%	18.59%	17.95%	17.17%
	$\chi_{1+2+3+4}$	6.38%	9.84%	7.87%	9.69%	14.86%	14.39%
RMSD	average	2.31Å	1.95Å	2.06Å	1.83Å	1.90Å	2.14Å
	standard deviation	0.20Å	0.17Å	0.21Å	0.19Å	0.18Å	0.15Å

Table 2. Percent correct prediction rate of side-chain χ-angles (within 40° deviation) and RMSD (λ = 0.9): NAT-SCWRL4SET

		BetaSCPWeb (A)				CISRR (b)	SCWRL4 (c)
		I (a1)	I + II (a2)	I + III (a3)	I + II + III (a4)		
χ	χ_1	78.96%	61.98%	55.90%	50.38%	85.16%	85.72%
	χ_{1+2}	58.80%	57.59%	33.65%	37.81%	72.69%	72.90%
	χ_{1+2+3}	20.25%	21.47%	10.89%	14.71%	35.12%	36.96%
	$\chi_{1+2+3+4}$	16.59%	15.97%	7.66%	11.47%	30.57%	30.88%
RMSD	average	2.11Å	1.79Å	2.16Å	1.94Å	1.56Å	1.87Å
	standard deviation	0.21Å	0.18Å	0.19Å	0.18Å	0.20Å	0.15Å

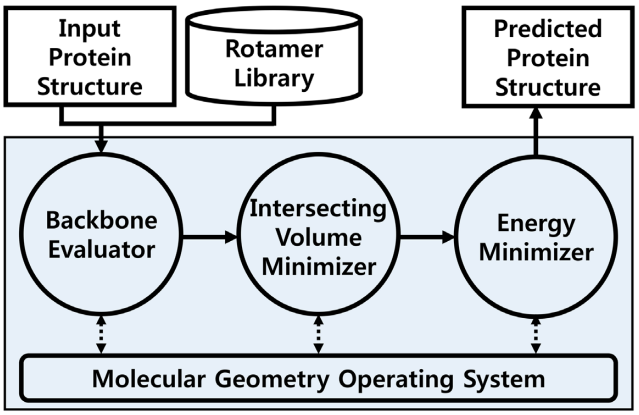

Figure 5. The architecture and computational flow of BetaSCPWeb.

Figure 6. The actualization of a PDB structure file fetched from RCSB PDB web site upon user's request.

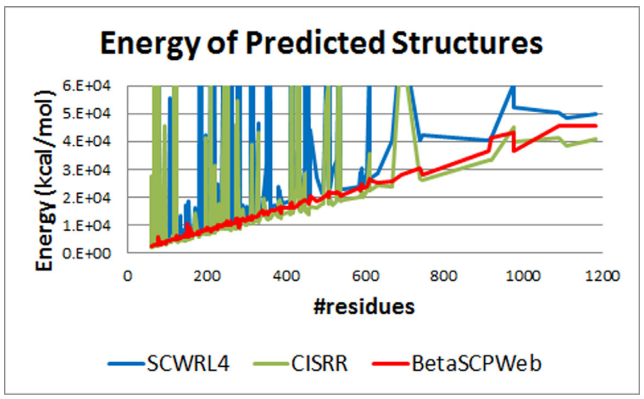

Figure 7. Benchmark with SCWRL4 and CISRR using NAT-SCWRL4SET and the backbone-dependent rotamer library (10) ($\lambda = 0.9$): (**A**) potential energy: BetaSCPWeb gives consistently lower energies. (**B**) Computation time: BetaSCPWeb uses slightly more computation than SCWRL4 but less than CISRR.

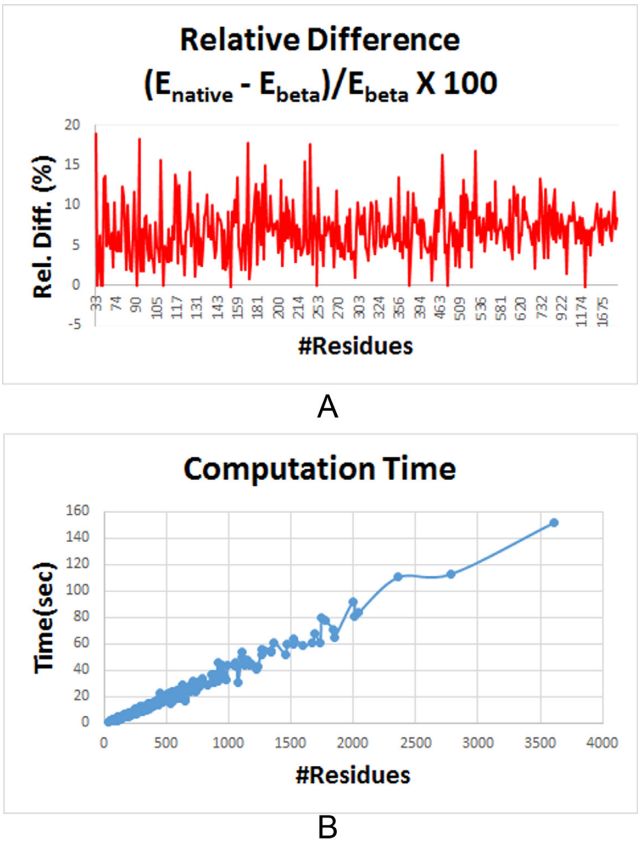

Figure 8. Performance of BetaSCPWeb on the CASP datasets from CASP rounds 6 to 11: (**A**) energy improvement from the native structure: BetaSCPWeb improves (i.e. lowers) the potential energy of native structures by ~7% on average. (**B**) Computation time as a function of protein size.

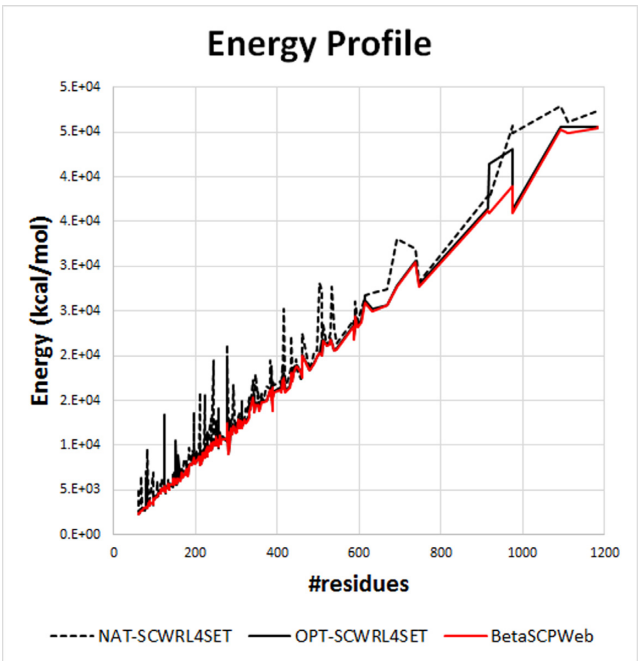

Figure 9. Energy profile of NAT-SCWRL4SET (the black dotted), OPT-SCWRL4SET (the black solid) and the structure predicted by BetaSCPWeb (the red; $\lambda = 0.9$) using the backbone-dependent rotamer library (10). Note the several high peaks of the native structures and the similarity of the optimized native structures and those predicted by BetaSCPWeb.

in OPT-SCWRL4SET and NAT-SCWRL4SET. The average μ and standard deviation σ were as follows: For $\Delta\chi_1$, $(\mu, \sigma) = (36.3^\circ, 44.5^\circ)$; For $\Delta\chi_2$, $(40.8^\circ, 43.0^\circ)$; For $\Delta\chi_3$, $(33.0^\circ, 39.9^\circ)$; For $\Delta\chi_4$, $(27.9^\circ, 34.6^\circ)$. We also computed the standard percent correct side-chain angles between OPT-SCWRL4SET and NAT-SCWRL4SET (i.e. the percentage of angles within the 40° degree variation, frequently used in the literature) in absolute accuracy values (16) as follows. $\chi_1 = 61.0\%$, $\chi_{1+2} = 54.0\%$, $\chi_{1+2+3} = 38.0\%$, and $\chi_{1+2+3+4} = 39.0\%$. The distribution of RMSD had an average of 1.62Å and standard deviation 0.18Å, where each RMSD was measured between the corresponding atoms in the corresponding structures of OPT-SCWRL4SET and NAT-SCWRL4SET. This experiment shows that the energy-optimized native structures are somewhat different from the native structures. Thus we use both the energy-optimized and the native structures as references for assessing the quality of the side-chains predicted by BetaSCPWeb.

Table 1 is the summary of the percent correct prediction rate of the predicted side-chains from the reference structure OPT-SCWRL4SET. The entries are absolute accuracies. The column A, B and C correspond to BetaSCPWeb, CISRR and SCWRL4, respectively. In column A, there are four subcolumns: A1 is the result after only Step I (i.e. the initial rotamer assignment) of the BetaSCP algorithm is applied, A2 after Step I and II are applied, A3 after Step I and III are applied and A4 after Step I, II and III are all applied. The prediction capability substantially improves in the given order. In particular, A4 sacrifices the prediction rate of χ_1 a little bit to increase the prediction rates of all χ_{1+2}, χ_{1+2+3}, and $\chi_{1+2+3+4}$. The RMSD significantly decreases from A1 to A4. The prediction power of BetaSCPWeb is significantly superior to those of both CISRR and SCWRL4 from the view points of both angular distribution and RMSD. Table 2 shows a similar analysis using NAT-SCWRL4SET as the reference structure and reveals a different prediction quality to that shown in Table 1. From the point of view of the native structure, the prediction powers of both CISRR and SCWRL4 are significantly superior to that of BetaSCPWeb when Step I, II and III are all applied. Note that BetaSCPWeb with Step I only (i.e. column 'a1' in Table 2) has quite a good prediction rate. Therefore, we designed BetaSCPWeb so that it can output two instances of a structure prediction: one after only Step I is applied (for the native structure preference) and the other after Step I, II and III are all applied (for the optimized structure preference).

The value of the empirical parameter λ in the attractive force, thus called an attraction scaling factor, should be determined. As the BetaSCP algorithm does not consider the attraction force when two atoms intersect, having $\lambda = 1.0$ leads to a substantial gap in the LJ-potential function between two atoms. To compensate the repulsive term of the LJ-potential, BetaSCPWeb currently uses $\lambda = 0.9$.

Handling missing atoms in BetaSCPWeb

Many protein structure files in PDB have missing atoms from either backbone or side-chain and thus it is critical for a web server to be prepared for such cases. BetaSCPWeb handles missing atoms as follows. If a backbone has one or more missing oxygen atoms, BetaSCPWeb predicts the location of the oxygen atoms and performs the SCP computation. The prediction is done by checking the geometric configuration of consecutive peptide planes, the bond lengths, and the angles of two consecutive bonds. If any atom other than oxygen is missing from a backbone, BetaSCPWeb does not perform any computation but produces a warning message so that users can be informed to correct the submitted structure file. If the beta carbon for the side-chain is missing, we choose one of the two possible locations of the atom which has a smaller intersection volume with the other atoms in the Euclidean neighborhood. However, if all the atoms in both main- and side-chains of a residue are missing (i.e. a residue is totally missing), BetaSCPWeb still produces a result assuming that the residue does not exist.

CONCLUSION

The BetaSCPWeb server efficiently predicts accurate protein side-chain structures that are close to their optimal conformation. Due to the NP-hardness of the SCP-problem, a heuristic algorithm is necessary. The one used in BetaSCPWeb employs the Voronoi diagram of atoms, its quasi-triangulation and beta-complex whose mathematical/computational properties are theoretically proven. BetaSCPWeb outperforms popular programs in terms of solution quality with a comparable computational time requirement. We are planning to enhance the algorithm in the near future by the incorporation of a flexible backbone and mutated amino acids.

FUNDING

Hanyang University [HY-2012 to J.R., D.-S.K.]; National Research Foundation of Korea (Basic Science Research Program) [2015R1D1A1A01061361 to J.R., M.L., J.C., D.-S.K.]; National Research Foundation of Korea (Biomedical technology development) [2015M3A9B5029741 to S.E.R.].
Conflict of interest statement. None declared.

REFERENCES

1. Dahiyat,B.I. and Mayo,S.L. (1997) De novo protein design: fully automated sequence selection. *Science*, **278**, 82–87.
2. Ashworth,J., Havranek,J.J., Duarte,C.M., Sussman,D., Monnat,R.J. Jr, Stoddard,B.L. and Baker,D. (2006) Computational redesign of endonuclease DNA binding and cleavage specificity. *Nature*, **441**, 656–659.
3. Chinea,G., Padron,G., Hooft,R., Sander,C. and Vriend,G. (1995) The use of position-specific rotamers in model building by homology. *Proteins*, **23**, 415–421.
4. Sanchez,R. and Šali,A. (1997) Advances in comparative protein-structure modelling. *Curr. Opin. Struct. Biol.*, **7**, 206–214.
5. Xiang,Z. and Honig,B. (2001) Extending the accuracy limits of prediction for side-chain conformations. *J. Mol. Biol.*, **311**, 421–430.
6. Althaus,E., Kohlbacher,O., Lenhof,H.-P. and Müller,P. (2002) A combinatorial approach to protein docking with flexible side chains. *J. Comput. Biol.*, **9**, 597–612.
7. Gray,J.J., Moughon,S., Wang,C., Schueler-Furman,O., Kuhlman,B., Rohl,C.A. and Baker,D. (2003) Protein-protein docking with simultaneous optimization of rigid-body displacement and side-chain conformations. *J. Mol. Biol.*, **331**, 281–299.
8. Dunbrack,R.L. Jr and Cohen,F.E. (1997) Bayesian statistical analysis of protein side-chain rotamer preferences. *Protein Sci.*, **6**, 1661–1681.

9. Lovell,S.C., Word,J.M., Richardson,J.S. and Richardson,D.C. (2000) The penultimate rotamer library. *Proteins*, **40**, 389–408.
10. Shapovalov,M.V. and Dunbrack,R.L. Jr (2011) A smoothed backbone-dependent rotamer library for proteins derived from adaptive kernel density estimates and regressions. *Structure*, **19**, 844–858.
11. Akutsu,T. (1997) Np-hardness results for protein side-chain packing. *Genome Informatics*, **8**, 180–186.
12. Desmet,J., Maeyer,M.D., Hazes,B. and Lasters,I. (1992) The dead-end elimination theorem and its use in protein side-chain positioning. *Nature*, **356**, 539–542.
13. Goldstein,R.F. (1994) Efficient rotamer elimination applied to protein side-chains and related spin glasses. *Biophys. J.*, **66**, 1335–1340.
14. Chazelle,B., Kingsford,C. and Singh,M. (2004) A semidefinite programming approach to side chain positioning with new rounding strategies. *Inform. J. Comput.*, **16**, 380–392.
15. Kingsford,C.L., Chazelle,B. and Singh,M. (2005) Solving and analyzing side-chain positioning problems using linear and integer programming. *Bioinformatics*, **21**, 1028–1036.
16. Krivov,G.G., Shapovalov,M.V. and Dunbrack,R.L. Jr (2009) Improved prediction of protein side-chain conformations with SCWRL4. *Proteins*, **77**, 778–795.
17. Miao,Z., Cao,Y. and Jiang,T. (2011) RASP: rapid modeling of protein side chain conformations. *Bioinformatics*, **27**, 3117–3122.
18. Tuffery,P., Etchebest,C., Hazout,S. and Lavery,R. (1993) A critical comparison of search algorithms applied to the optimization of protein side-chain conformations. *J. Comput. Chem.*, **14**, 790–798.
19. Tuffery,P., Etchebest,C., Hazout,S. and Lavery,R. (1991) A new approach to the rapid determination of protein side chain conformations. *J. Biomol. Struct. Dyn.*, **8**, 1267–1289.
20. Ryu,J. and Kim,D.S. (2013) Protein structure optimization by side-chain positioning via beta-complex. *J. Glob. Optim.*, **57**, 217–250.
21. Ryu,J., Lee,M., Cha,J., Song,C. and Kim,D.S. (2014) BetaSCP2: a program for the optimal prediction of side-chains in proteins. *Lecture Notes in Computer Science*, **8592**, 333–340.
22. Kim,D.S., Cho,Y. and Kim,D. (2005) Euclidean Voronoi diagram of 3D balls and its computation via tracing edges. *Comput. Aided Des.*, **37**, 1412–1424.
23. Kim,D.-S., Cho,Y., Sugihara,K., Ryu,J. and Kim,D. (2010) Three-dimensional beta-shapes and beta-complexes via quasi-triangulation. *Comput. Aided Des.*, **42**, 911–929.
24. Okabe,A., Boots,B., Sugihara,K. and Chiu,S.N. (1999) *Spatial Tessellations: Concepts and Applications of Voronoi Diagrams*, 2nd edn. John Wiley & Sons, Chichester.
25. Kim,D.-S., Kim,D., Cho,Y. and Sugihara,K. (2006) Quasi-triangulation and interworld data structure in three dimensions. *Comput. Aided Des.*, **38**, 808–819.
26. Kim,D.-S., Cho,Y. and Sugihara,K. (2010) Quasi-worlds and quasi-operators on quasi-triangulations. *Comput. Aided Des.*, **42**, 874–888.
27. Kim,J.-K., Cho,Y., Kim,D. and Kim,D.-S. (2014) Voronoi $\mathbb{R}^2$ (balls and ellipsoids) diagrams, quasi-triangulations, and beta-complex for disks in $\mathbb{R}^2$: The theory and implementation in BetaConcept. *J. of Comput. Des. and Eng.*, **1**, 79–87.
28. Weizi,E. (1991) Smallest enclosing disks (balls and ellipsoids). *Lecture Notes in Computer Science*, **555**, 359–370.
29. Wang,C., Schueler-furman,O. and Baker,D. (2005) Improved side-chain modeling for protein-protein docking. *Protein Sci.*, **14**, 1328–1339.
30. JSmol: an open-source HTML5 viewer for chemical structures in 3D, http://wiki.jmol.org/index.php/JSmol.
31. Cao,Y., Song,L., Miao,Z., Hu,Y., Tian,L. and Jiang,T.(2011) Improved side-chain modeling by coupling clash-detection guided iterative search with rotamer relaxation. *Bioinformatics*, **27**, 785–790.